Article

Novel Insights of Herbal Remedy into NSCLC Suppression through Inducing Diverse Cell Death Pathways via Affecting Multiple Mediators

Uyanga Batbold [1] and Jun-Jen Liu [1,2,3,*]

1   Ph.D. Program in Medical Biotechnology, College of Medical Science and Technology, Taipei Medical University, Taipei 11031, Taiwan; uyanga.gemini@yahoo.com
2   School of Medical Laboratory Science and Biotechnology, College of Medical Science and Technology, Taipei Medical University, Taipei 11031, Taiwan
3   Traditional Herbal Medicine Research Center, Taipei Medical University Hospital, Taipei 11031, Taiwan
*   Correspondence: jjliu_96@tmu.edu.tw

Abstract: Artemisia species previously have been reported to have antimicrobial, antioxidant, antiulcer, and anticancer properties. In this study, we investigated the prospective antitumor effects of *Artemisia santolinifolia* ethanol extract (ASE) against two non-small cell lung cancer (NSCLC) cell lines and their molecular mechanisms of action. Morphological observations and flow cytometric analyses showed that ASE induced cell death in A549 and H23 cells but with different action features. Further studies by Western blotting showed that ASE induced caspase-3 cleavage in H23 cells, suggesting caspase-dependent apoptosis was predominantly involved in H23 cell death. Contrarily, ASE treatment selectively altered the glutathione peroxidase (GPX4) protein expression, reactive oxygen species (ROS) generation, and lipid peroxidation in A549 cells, all of which are linked to ferroptosis. Using a ferroptosis inhibitor (desferrioxamine (DFO)), further study showed that DFO could significantly rescue ASE-induced cell death. All these results implied that ASE induced ferroptosis predominately in A549 cells. Several studies have demonstrated that the nuclear factor erythroid 2–related factor 2 (NRF2) can be dual-selectively targeted depending on the cell line. Subsequently, it can exert opposing effects until either being activated or suppressed. This was consistent with our data, which might explain inconsistent observations of the cell death type in this study. In addition, after ASE treatment, signal transduction and activator of transcription 3 (STAT3) were inhibited in both cell lines. Consequently, downstream prosurvival proteins, including heat shock protein 70 (HSP70) and survivin, which play pivotal roles in the STAT3 pathway, decreased after ASE administration. Our findings revealed that ASE inhibited NSCLC cell proliferation by simultaneously downregulating prosurvival protein expressions and activating multiple cell death pathways.

Keywords: *Artemisia santolinifolia*; ferroptosis; apoptosis; NRF2; STAT3

1. Introduction

Lung cancer causes more than 25% of cancer-related mortality among all cancer types, and 80% of these lung cancer cases are non-small cell lung cancer (NSCLC) [1]. Besides, lung cancer's 5-year relative survival rate is comparatively low than the other leading cancer sites (17.4%) [2]. The two main aspects that restrict the efficacy of chemotherapy are its toxicity [3] and the development of resistance [4]. Particularly in the advanced stages of lung cancer, chemotherapeutic drug resistance cannot achieve adequate results and is the primary factor considered to cause more than 90% of treatment failures [5]. Traditional medicine utilizes the broad-spectrum pharmacological effects of multiple ingredients to influence multiple targets [6]. With clinical applications and evidence gathered over thousands of years, traditional medicine has recently attracted increasing attention for its effectiveness and fewer side effects [7]. In recent years, with the advancement of translational science and

molecular biology, herbal remedies and combinational formulas are being tested in both preclinical and clinical trials as viable treatment options for various malignancies [8]. Thus, it might be advantageous to identify and develop natural compounds, active ingredients, single herbs and combinational formulas in traditional medicine that could influence diverse signaling pathways on the tumor while minimizing side effects compared to other conventional therapies.

Artemisia santolinifolia is one of the species of the genus *Artemisia* that forms a monodominant shrub layer common in stony or disturbed lower-montane sites throughout Central Asia south of the Himalayas [9]. The genus *Artemisia*, often known collectively as wormwood, is a large and diverse genus belonging to the daisy family Asteraceae and encompasses around 500 species of herbs and shrubs [10–12]. They are frequently used to treat hepatitis, diabetes, malaria, laryngitis, pharyngitis, hemorrhaging, rheumatoid arthritis, and fungal, bacterial, and viral infections [11,13–18]. Although *A. santolinifolia* is ubiquitous in Central Asia, very few studies have been conducted on this species, and its biology is poorly known [19]. In addition, the anticancer activities of other *Artemisia* species, including *A. vulgaris* in human colon cancer cells, *A. scoparia* against NSCLC cell line, and *A. aucheri* and *A. annua* extracts have also been scientifically validated [20–23]. However, the antiproliferative role of *A. santolinifolia* in NSCLC and the possible underlying mechanisms have not yet been reported.

This study aimed to shed light on the mechanisms of action of ASE toward NSCLC. With a motivation to elucidate the characterization changes that occurred in NSCLC responsible for ASE anticancer activity upon exposure, microscopic visualization and flow cytometric analysis were performed. Additionally, the corresponding gene expression changes related to the distinct patterns of cell death were assessed using Western blot analysis. Here, our group reports the selectivity ASE in triggering diverse cell death modes via affecting multiple mediators for the first time. We hypothesized that the anticancer properties of ASE may be due to the inhibition of pro-survival protein expressions in NSCLC.

2. Materials and Methods

2.1. Antibodies and Reagents

Chemical reagents, including desferrioxamine (DFO), sulforhodamine B (SRB), dichlorofluorescein diacetate (DCFH-DA), propidium iodide (PI), ribonuclease A (RNase A), and trichloroacetic acid (TCA), were obtained from Sigma-Aldrich (St. Louis, MO, USA), while the Annexin V FITC-Apoptosis Detection Kit was obtained from Biolegend (San Diego, CA, USA) and C11-BODIPY 581/591 was obtained from Cayman Chemical (Ann Arbor, MI, USA). Antibodies including anti-heat shock protein 70 (HSP70), nuclear factor erythroid 2–related factor 2 (NRF2), glutathione peroxidase (GPX4), goat anti-mouse immunoglobulin G (IgG)-horseradish peroxidase (HRP), and donkey anti-rabbit IgG-HRP were obtained from Gentex (Irvine, CA, USA), while antibodies against β-actin, signal transducer and activator of transcription 3 (STAT3), and phosphorylated (p)-STAT3 were purchased from Abcam (Cambridge, UK). Antibodies against caspase-3 and survivin were obtained from Cell Signaling Technology (Danvers, MA, USA).

2.2. ASE Materials and Extraction

Artemisia santolinifolia (provisionally accepted name: Artemisia santolinifolia Turcz. ex Besser; synonym: Artemisia santolinifolia subsp. Santolinifolia, Artemisia gmelinii Weber ex Stechm.) is a "wormwood" semi-shrub with three-pinnatisect leaves that are widely found from Central Asia to Eastern Europe. There are 400 to 500 different types of this species. The herb name has been checked in http://www.theplantlist.org and http://www.catalogueoflife.org databases, accessed on 20 September 2020, where the plant name is an accepted name in the genus Artemisia with one star. The record derives from The International Compositae Alliance (TICA), which reports it as with original publication details: Nouv. Mém. Soc. Imp. Naturalistes Moscou 3: 87 (1834). Air-dried A. santolinifolia

was provided by Mong-Em (Traditional herb medicine company; Ulaanbaatar, Mongolia). The sample was collected in Omnogobi, Gurvansaikhan (Mongolia), August 2020. Dried herbs were extracted in ethanol (1:1 *w/v*) with sonication for 6 h at 60 °C. Afterward, the supernatant was filtered through filter paper to remove solid particles. A rotavapor (Buchi Labortechnik, Flawil, Switzerland) subsequently removed the ethanol of the alcoholic extract at 40 °C. Finally, for the in vitro and cell culture experiments, the dried herbal extracts were dissolved in ethanol at various concentrations and diluted in culture media.

2.3. Cell Culture

The human A549 and H23 NSCLC cell lines were purchased from the ATCC Cell Bank (Manassas, VA, USA) and cultured in Dulbecco's modified Eagle medium (DMEM)/F12 and RPMI 1640 supplemented with 10% heat-inactivated fetal bovine serum (FBS) in the presence of 1% L-glutamine and a 100 U/mL of a 1% penicillin-streptomycin solution. Cells were grown at 37 °C in a 5% CO_2 humidified incubator before use in experiments.

2.4. Cell Cytotoxicity Assay

The antiproliferative effects of the ASE were determined with an SRB assay adapted from a previous publication [24]. Briefly, A549 and H23 cells were plated at respective concentrations of 2500 and 3000 cells/well in 96-well plates. After incubation overnight, cells were treated with different concentrations of ASE (10–400 µg/mL) for 24, 48, and 72 h. At the end of the exposure periods, ice-cold TCA was applied to fix them after the cells had been rinsed twice with phosphate-buffered saline (PBS). Cells were stained with SRB for 1 h and followed with three washes with a 1% acetic acid solution. A Tris-based solution was used to solubilize the plate after air-drying. The absorbance value for each well was measured on a SpektraMax iD3 multi-mode microplate reader (Molecular Devices, Silicon Valley, CA, USA).

2.5. Cell Staining

Changes in cell morphologies were evaluated with Liu's stain [25]. Briefly, 18-mm slides were placed in six-well plates prior to cell seeding. The following day, cells were treated with ASE for 24, 48, and 72 h. Afterward, cells were washed with PBS, sequentially stained with Liu A followed by Liu B. Then, slides were gently washed with distilled water and air-dried for cell morphological observations. Photographs were taken with a digital camera (Leica, Wetzlar, Germany).

2.6. Apoptosis Analysis

In this study, FITC-conjugated Annexin V and 7-aminoactinomycin D (7-AAD) apoptosis detection kits were used to detect apoptosis. Cells were exposed to DFO, a high-affinity Fe (III) chelator, at a concentration of 100 µM for 12 h prior to ASE treatment, alone or in combination with 100 or 200 µg/mL of the ASE for 24 h. At the end of treatment, cells were harvested by trypsinization (0.25%, Trypsin-EDTA) and resuspended in a binding buffer followed by staining with FITC-conjugated anti-Annexin V and 7-AAD for 20 min. Cell death was analyzed with an Attune NxT flow cytometer (Invitrogen, Carlsbad, CA, USA), and early and late apoptosis rates were measured using FlowJo software (TreeStar, Ashland, OR, USA).

2.7. Analysis of ROS

To detect intracellular ROS levels, we used the DCFH-DA method. Briefly, cells were seeded in six-well plates at a density of 5×10^5 cells/well, cultured overnight, and then treated with 100 or 200 µg/mL of the ASE combined with or without 100 µM DFO for 4, 8, and 24 h. At the end of treatment, cells were collected and incubated with 5 µM DCFH-DA for 30 min in an incubator. The fluorescence intensity of cells was analyzed by flow cytometry. Data analysis was performed using FlowJo software (TreeStar).

2.8. Analysis of Lipid ROS

Lipid ROS were stained with C11-BODIPY 581/591 and analyzed using flow cytometry as previously described [26]. Briefly, after appropriate treatment, cells were incubated with 2 μM C11-BODIPY 581/591 in a culture medium for 1 h and then washed with PBS. Cells were harvested by trypsinization (0.25%, Trypsin-EDTA) and collected, and flow cytometry was used to assess the fluorescence intensity of cells. Data analysis was performed using FlowJo software (TreeStar).

2.9. Western Blot Analysis

Briefly, A549 and H23 cells were seeded in 60-mm dishes and incubated overnight. Afterward, cells were treated with the ASE at a 100 or 200 μg/mL concentration for 48 h. Treated cells were collected and lysed in RIPA buffer. Each sample with 30 μg of total protein was separated via electrophoresis on 10% or 12% sodium dodecylsulfate (SDS)-polyacrylamide gels and transferred onto nylon membranes. Membranes were blocked with 5% skim milk containing Tris-buffered saline (TBS) buffer, then primary antibodies were added to the samples (containing 5% milk). After washing twice with a TBS buffer, the primary antibody was detected with a goat anti-rabbit or rabbit anti-mouse secondary antibody. Finally, proteins were analyzed with a chemiluminescent detection kit and exposed for 1~60 s in ImageQuant (LAS 4000 series).

2.10. Liquid Chromatography (LC)-Tandem Mass Spectrometric (MS/MS) Analysis

The analytical LC-MS/MS experiment was performed on a Waters Acquity UPLC (Ultra-performance liquid chromatography) I-Class system and Vion IMF QToF (quadrupole time of flight) MS spectrophotometer. The system was equipped with a Waters BEH C18 Acquity analytical column (75 μm × 150 mm, 1.8 μm). A temperature of 40 °C was set in the column oven and a temperature of 4 °C was set for the autosampler. For each LC-HDMSE run, approximately 2 μL of the sample (1 mg/mL) was loaded onto the column through a 10 μL sample loop using 98% of mobile phase A (0.1% formic acid in H_2O) at a flow rate of 0.4 mL/min with gradient elution consisting of an increasing the mobile phase B from 20% to 46% (0.1% formic acid in acetonitrile (ACN)) over 30 min, followed by a re-equilibration step at 20% of the mobile phase B for 10 min and was delivered to the reference sprayer of the LockSpray source.

The positive-mode electrospray ionization (ESI) using a LockSpray source was utilized for all analyses. The calibration was performed with a leucine enkephalin solution (200 fmol/μL). Accurate LC-HDMSE mass data were acquired in low-energy (MS) and high-energy (MSE) modes of acquisition with parameters set as follows: a mass scan range of m/z 50 to 1000, the capillary voltage of 2 kV, the temperature of 150 °C, and a cone voltage of 30 V.

2.11. Statistical Analysis

All statistical analyses were performed using Sigmaplot software (Systat Software, San Jose, CA, USA). Data are represented as means ± standard error (SE). Differences between the two groups were calculated using the Student's *t*-test and analysis of variance (ANOVA) with pair-wise comparisons. * $p < 0.05$, ** $p < 0.01$, and *** $p < 0.001$ was considered statistically significant.

3. Results

3.1. ASE Inhibits A549 and H23 Cell Growth

We examined the cytotoxic effects of the ASE with an SRB assay to assess changes in the viability of the A549 and H23 cell lines. As shown in Figure 1A,B, ASE reduced cell viability in a dose- and time-dependent manner in both NSCLC cell lines. Values of the 50% inhibitory concentration (IC_{50}) of ASE in A549 and H23 cells were 206.6 and 213.4 μg/mL, respectively (Figure 1C). Hence, we used 100 and 200 μg/mL concentrations in subsequent experiments to determine concentration-dependent features of the ASE. Furthermore, a

morphological analysis by both phase-contrast microscopy and Liu's staining demonstrated that ASE-treated A549 cells in all three-time points first proceeded with cell shrinking followed by condensation of cytoplasmic constituents and a "ballooning" phenotype, which form of clear, spherical morphology (Figure 1D,E). These morphological features are similar to the phenotypical changes that occur during ferroptosis [27]. However, in contrast to A549 cells, no identical cell morphology changes were observed in H23 cells after ASE treatment. Instead, H23 cells preferentially displayed cell shrinkage, plasma membrane blebbing, and reduced cytoplasmic branches, which might indicate apoptosis hallmarks.

(A)

(B)
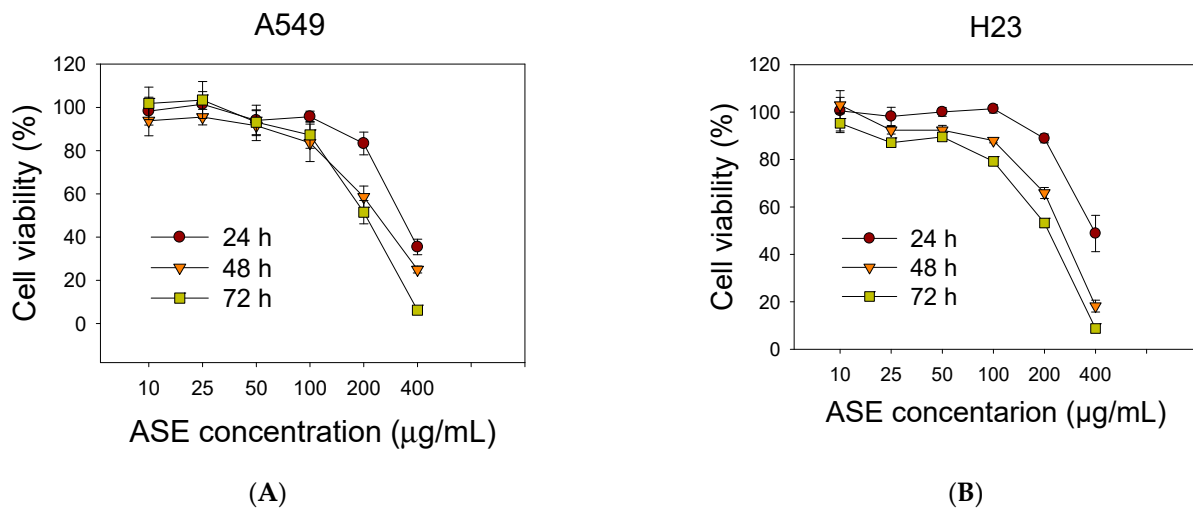
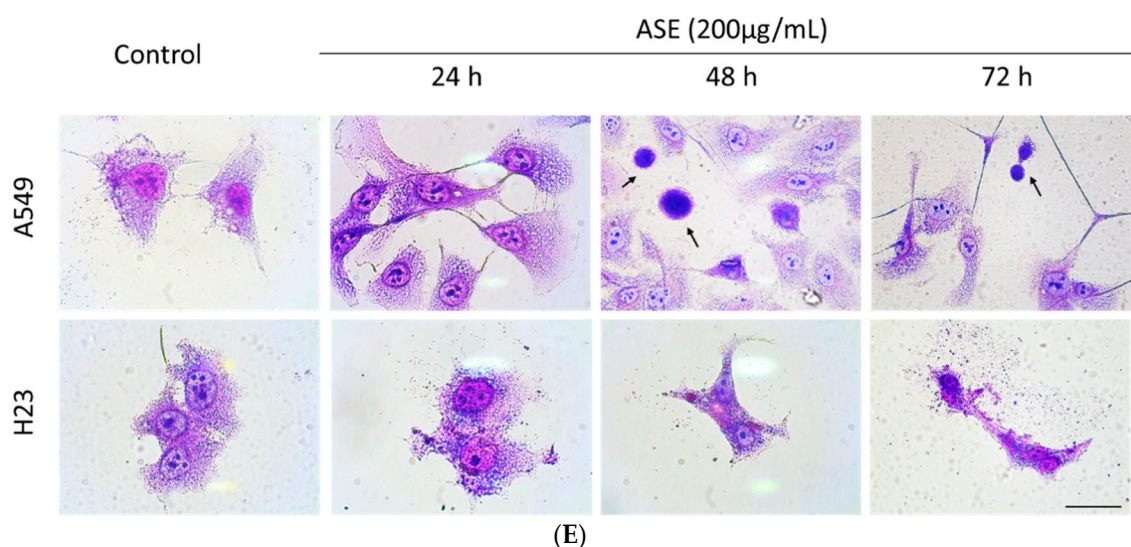| Cell Line	IC$_{50}$, µg/mL		
	24 h	**48 h**	**72 h**
A549	339.0	238.0	206.6
H23	394.2	266.7	213.4

(C)

(D)

Figure 1. *Cont.*

(E)
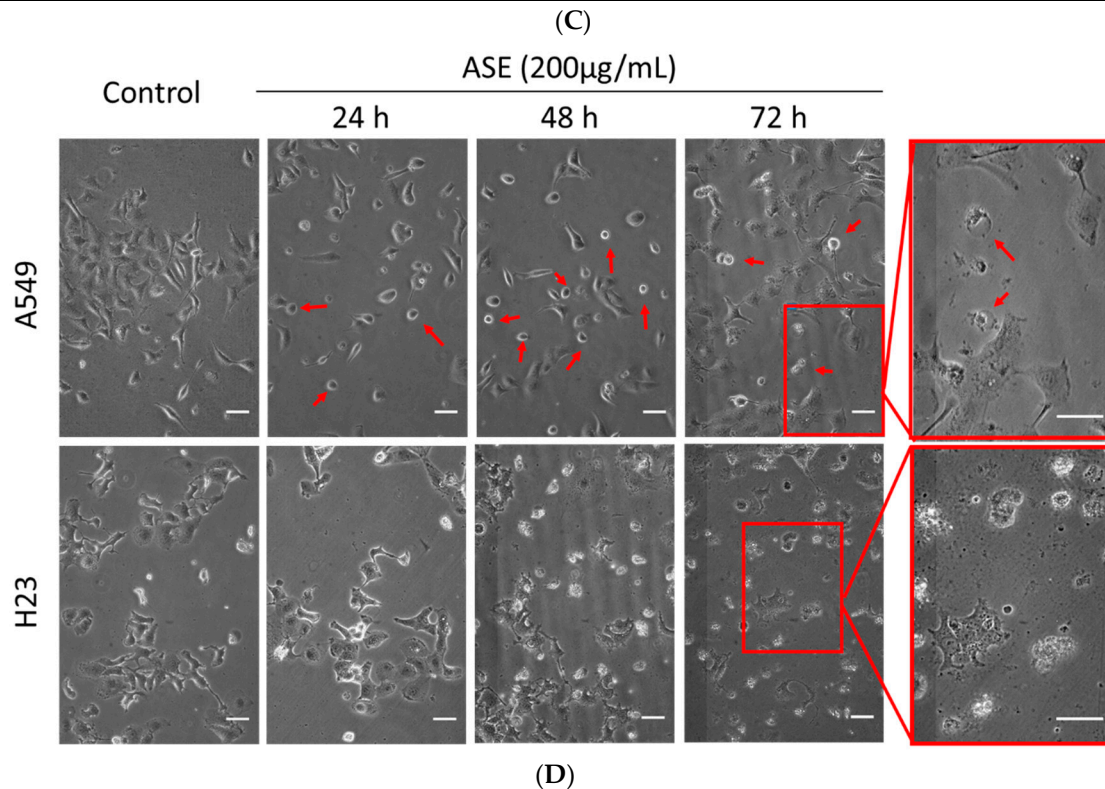
Figure 1. Effect of *Artemisia santolinifolia* ethanol extract (ASE) on cell growth of different non-small cell lung cancer (NSCLC) cell lines. Lung cancer cells were treated with different concentrations of the ASE for 24, 48, and 72 h. Cell viability of A549 (**A**) and H23 cells (**B**) was assessed by SRB assay. (**C**) The 50% inhibitory concentration (IC50) values were calculated at different time points. All data are the mean ± SE of three replicate experiments. (**D**) Light microscopic changes of cellular shape during ferroptosis. A549 and H23 cells were exposed for indicated durations to 200 μg/mL ASE and observed by phase-contrast microscopy. Ferroptotic cells, presenting a typical rounded "ballooning" phenotype morphology, are indicated by red arrowheads. (**E**) Morphological changes after ASE treatment evaluated with Liu's stain. Black arrows indicate a few examples of rounded, dying cells. Representative fields are shown. Scale bar = 50 μm.
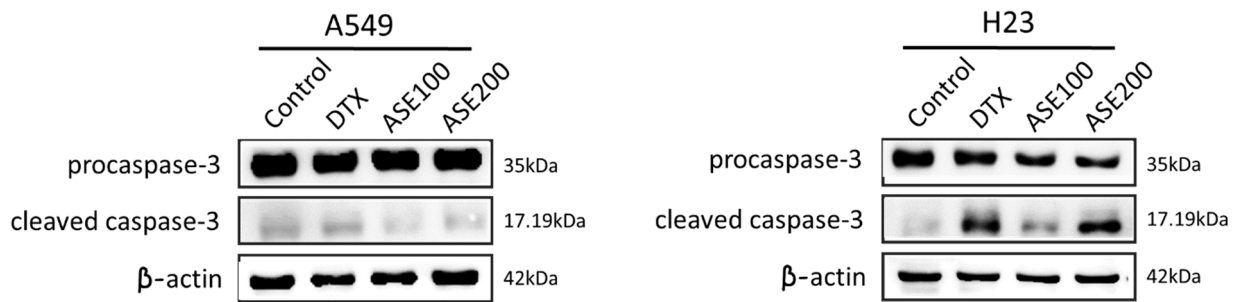
3.2. ASE Triggers Different Cell Death Features

Active ingredients of *Artemisia* species were shown to induce various cell death modes (apoptosis, autophagy, ferroptosis, necrosis, necroptosis, and oncosis) through downregulating specific signal transducers [28]. Thus, ASE's cytotoxicity toward NSCLC cells was evaluated by a flow cytometry analysis. The results of Annexin/7-AAD staining revealed that the ASE induced a dose-dependent increase in cell death but displayed different patterns in the two cell lines (Figure 2A). ASE treatment at the higher concentration caused A549 cells to cluster in the upper left quadrant (7-AAD+, Annexin V−) from 1.9% ± 0.7% to 34.8% ± 4.8%, whereas the apoptotic rate was significantly higher in the positive control group (Docetaxel (DTX)). In contrast, in H23 cells, ASE induced early and late apoptosis (in the right quadrant; Annexin V+) from 11.1% ± 3.3% to 28.9% ± 3.5% at the higher concentration of ASE. These results indicate that ASE triggered more apoptotic death in H23 cells, whereas A549 cells displayed a more necrotic form of cell death. This was consistent with the data analyzed in Figure 2B. This conclusion was proven by a Western blot analysis with the potential implication of apoptosis-related proteins, where the ASE (100 and 200 μg/mL) dose-dependently reduced procaspase-3 expression after 48 h, while concurrently increasing cleavage of caspase-3 in H23 cells (Figure 2C). In A549 cells, however, no significant change in procaspase-3 or cleaved caspase-3 levels was detected, even at the higher ASE dose (Figure 2D). These data suggest that the ASE may predominantly trigger caspase-dependent apoptosis in H23 cells as well as a caspase-independent non-apoptotic pathway in A549 cells. Consequently, both cell lines ultimately underwent cell destruction while concurrently showing distinct cell death features.

(**A**)

(**B**)
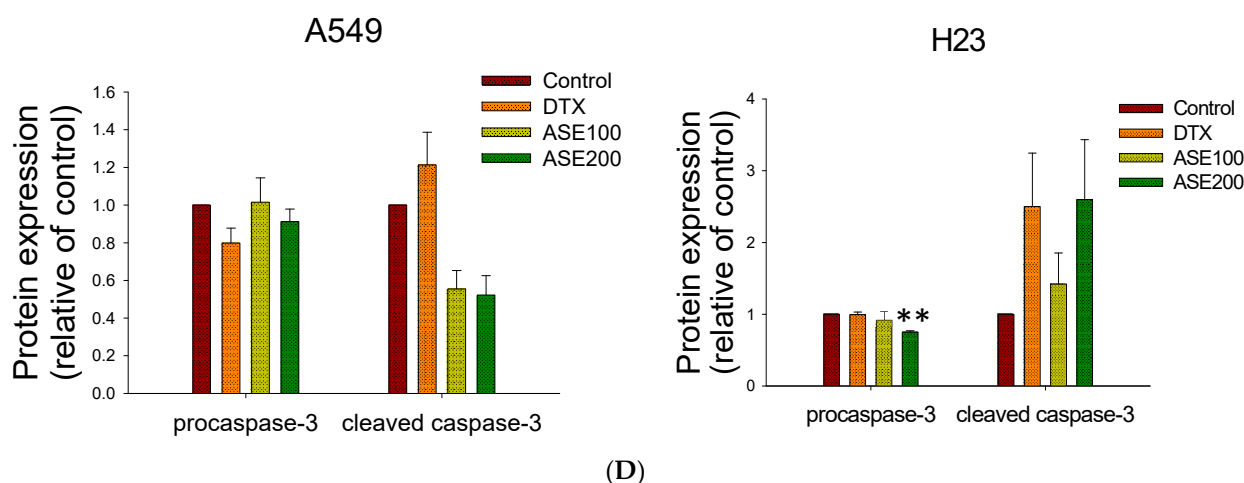

(**C**)

Figure 2. *Cont.*

(**D**)
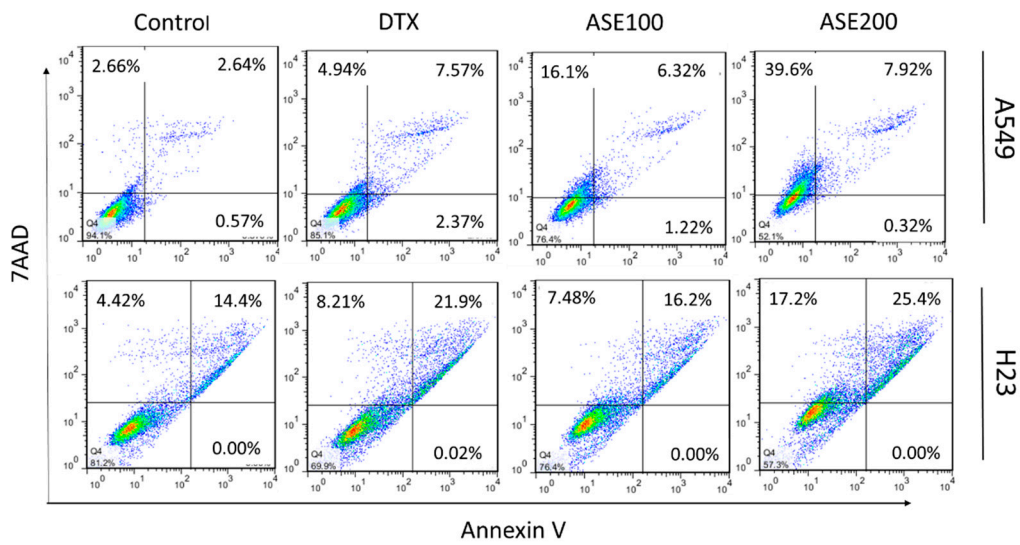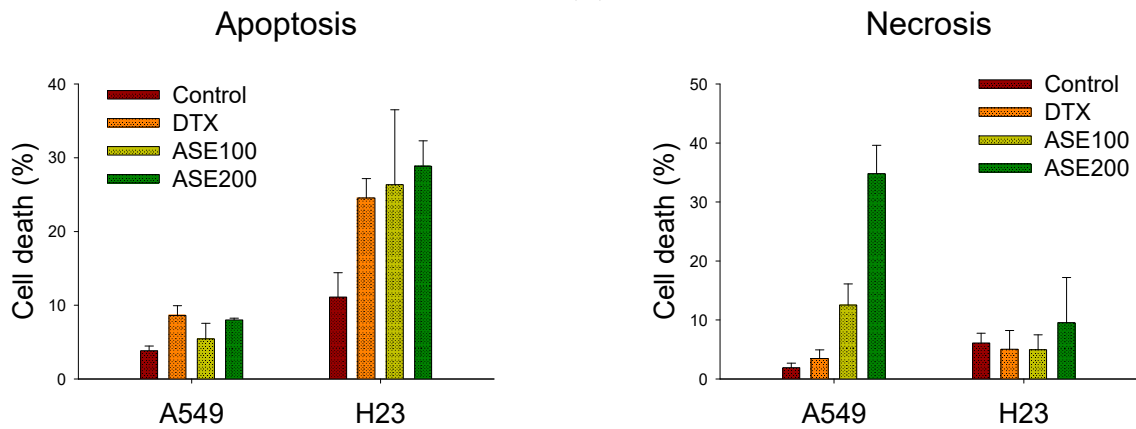
Figure 2. The ethanol extract of *Artemisia santolinifolia* (ASE) triggers different features of the cell death mode. Flow cytometry and Western blotting were performed to analyze the cell death mode following ASE and DTX treatment in A549 and H23 cells. (**A**) Apoptosis assay after staining with Annexin V-FITC/7-aminoactinomycin D (7-AAD). A549 and H23 cells were treated with 100 and 200 μg/mL ASE or 0.5 nM DTX (the positive control) for 48 h. (**B**) Quantification of dead cells following ASE treatment. (**C**) Representative images of Western blot analysis of caspase-3 expression with the most significant alterations. β-actin was used as a loading control. (**D**) Histograms quantified Western blot results of three replicates. Data are the mean ± SE; ** $p < 0.01$ vs. the corresponding control.

3.3. ASE Induced Ferroptosis Domineered in the A549 Cell Line

ROS accumulation and lipid peroxidation are both involved in ferroptosis, ultimately leading tumor cells to undergo oxidative cell death [29]. As mentioned above, A549 cells treated with the ASE for 48 h exhibited increased numbers of 7-AAD-positive cells distinct from those Annexin-V-positive cells in the positive control, the DTX group. In addition, by evaluating morphological changes, we determined that the ASE induced a spherical morphology configuration that prevailed in A549 cells (Figure 1D,E) which was similar to morphological changes of ferroptotic cells [27]. Therefore, both intracellular ROS levels and lipid peroxidation were analyzed using DFCH-DA and C11-BODIPY assays after exposure to the ASE. As expected, the ASE (100 and 200 μg/mL) triggered significant increases in ROS levels and lipid ROS activation preferentially in the A549 cell line but not in H23 cells (Figure 3A,C). Co-treatment of cells with the potent ferroptosis inhibitor, DFO, completely abrogated the ASE-induced population of ROS-positive cells and lipid peroxidation in A549 cells, but with no such effect in H23 cells (Figure 3A–C). Moreover, the results from Annexin/7-AAD double staining using a flow cytometric analysis showed that DFO could almost entirely rescue the ASE-induced cell death response in A549 cells, whereas it only partially reversed cell viability in H23 cells (Figure 3D). GPX4 was previously described as a crucial defense enzyme against lipid peroxidation, and the proper functioning of GPX4 is essential for cellular processes in preventing ferroptosis [30,31]. Hence, GPX4 expression after ASE treatment was evaluated. Results showed that the ASE decreased the GPX4 level at a significantly higher rate in ASE concentrations of 200 μg/mL, principally in the A549 cell line (Figure 3E,F) with statistical significance. Conversely, there was nearly no alteration in GPX4 levels in H23 cells, as shown in Figure 3E,F. Collectively, our data showed that non-apoptotic iron-dependent ferroptosis was primarily involved in A549 cell death but not in H23 cell death.
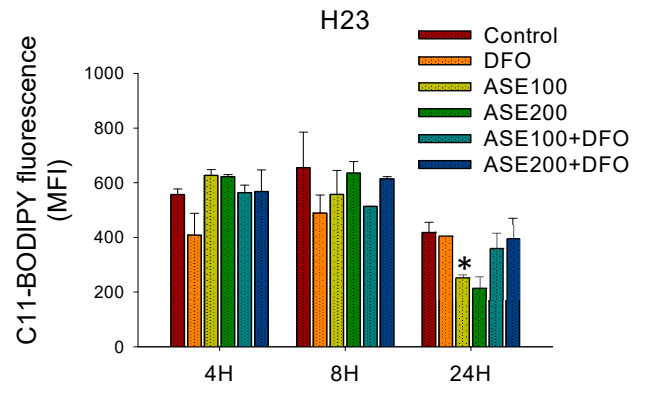
(**A**)

(**B**)

(**C**)

Figure 3. *Cont.*
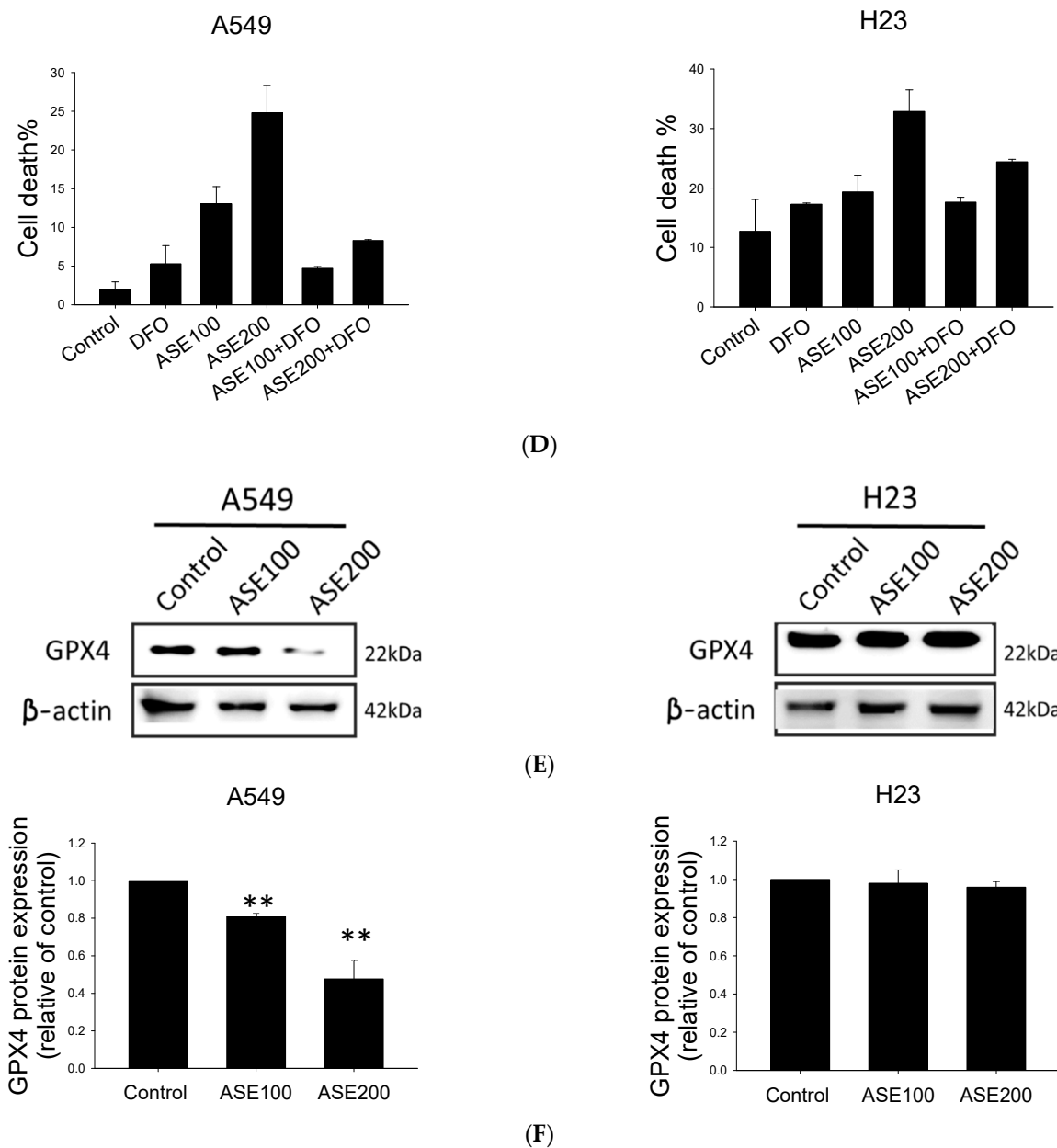
(D)

(E)

(F)
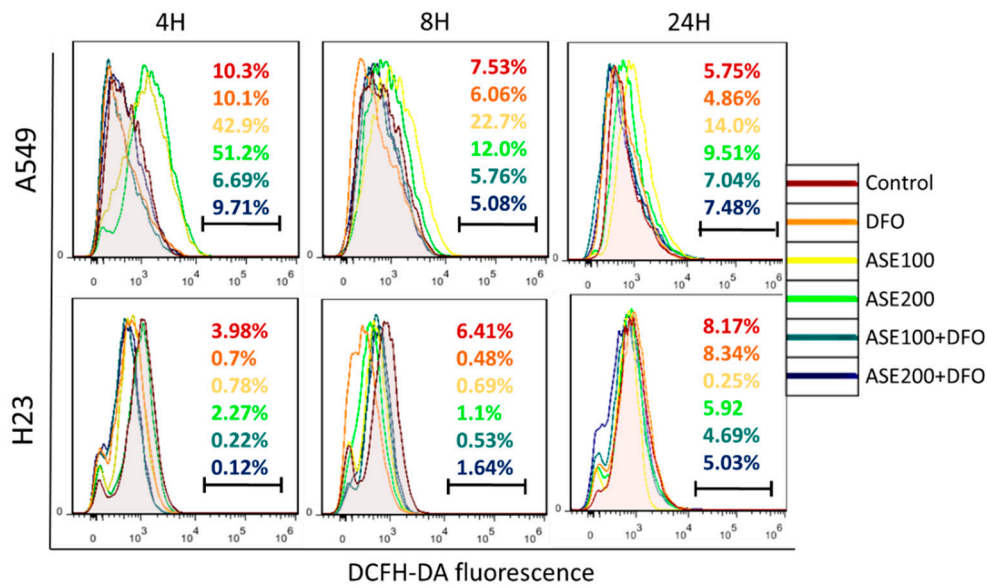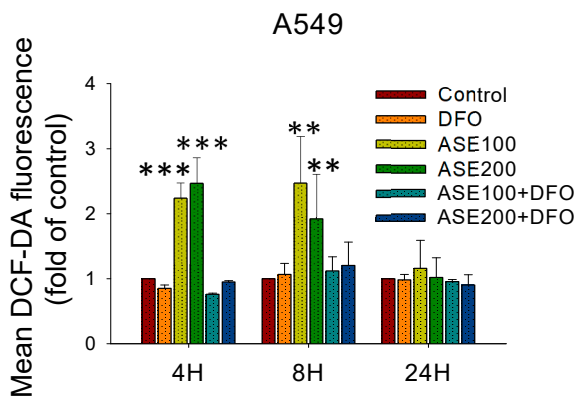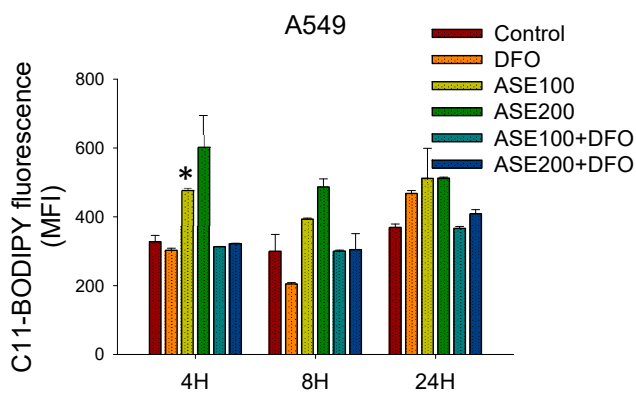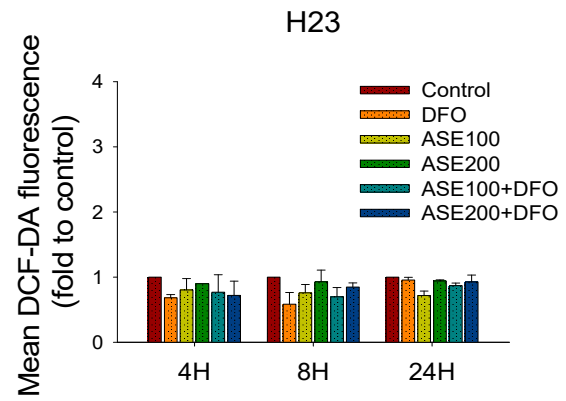
Figure 3. Treatment with the iron chelator, desferrioxamine (DFO), prevented ferroptosis upon response to exposure to the ethanol extract of *Artemisia santolinifolia* (ASE) in non-small cell lung cancer (NSCLC) cells. A549 and H23 cells were treated with DFO (100 µM) 12 h prior to ASE (100 and 200 µg/mL) treatment. (**A**) The ASE induced reactive oxygen species (ROS) production in A549 and H23 cells as determined by a DCFH-DA assay. (**B**) Histograms represent the effect of DFO on ASE-induced ROS production of three replicates (MFI, mean fluorescence intensity), and lipid ROS levels were measured using a C11-BODIPY assay after indicated treatment above (**C**). (**D**) Cell death populations of A549 and H23 cells following ASE treatment for 24 h in the presence or absence of the iron-chelator, DFO, as quantified by Annexin/7-AAD staining and analyzed using flow cytometry. (**E**) Glutathione peroxidase (GPX4) expression levels in A549 and H23 cells after treatment with the ASE at a concentration of 100 and 200 µg/mL for 48 h. Representative images of Western blot analysis of proteins with the most significant alterations. β-actin was used as a loading control. (**F**) Histograms of Western blot results of three replicates. Data are the mean ± SE; * $p < 0.05$, ** $p < 0.01$, *** $p < 0.001$ vs. the corresponding control.

3.4. ASE Dual-Selectively Targets the NRF2/STAT3 Axis and Suppresses Survivin and HSP70 Expressions

To investigate the mechanisms through which the ASE induces cell death, we evaluated expressions of prosurvival proteins in NSCLC cells after ASE exposure. According to the results of Wang's study [32], a major artemisinin derivative, dihydroartemisinin, significantly suppressed the phosphorylation of the STAT3 signaling molecule in colon cancer cell death. Furthermore, the previous study provided evidence that STAT3/NRF2 signaling might be involved in regulating ferroptosis by indicating that STAT3/NRF2 activation could enhance the antioxidant capacity of cells and protect against oxidative damage [33]. Thus, we analyzed NRF2 and STAT3 levels after ASE treatment in both cell lines. As shown in Figure 4, the ASE suppressed NRF2 expression mainly prevailed in A549 cells in a dose-dependent manner but slightly upregulated its expression in the H23 cell line. However, despite triggering multiple cell death modes, ASE strongly inhibited the STAT3 phosphorylation level in both A549 and H23 cell lines. At a 200 μg/mL concentration, respective inhibition rates of p-STAT3 were 61.5% ± 0.5% and 50.6% ± 0.1% in A549 and H23 cells with statistical significance (Figure 4B,C). Among known prosurvival proteins downstream of the STAT3 signaling molecule, HSP70 and survivin were shown to impact against apoptosis in tumor cells, and thus we further examined HSP70 and survivin protein levels after ASE treatment. As expected, HSP70 expression was downregulated by approximately 53.5% ± 0.05% at the indicated concentration in A549 cells, whereas it had decreased by 53.8% ± 0.07% in H23 cells at 48 h (Figure 4A,B). Statistically significant dose-dependent effects were also observed in survivin expression in both cell lines exposed to ASE. Collectively, dual-selective alteration of NRF2, which could be defined as regulatory crosstalk between two distinct forms of cell death, together with downregulation of p-STAT3 and the downstream prosurvival proteins in both cell lines suggests that ASE showed antitumor activity through attenuating the defense mechanisms of cells.
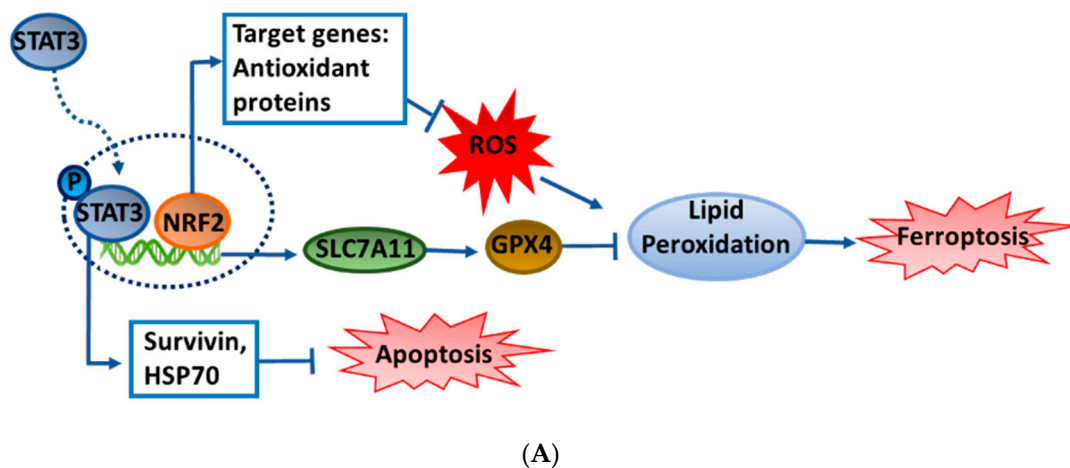

(**A**)

Figure 4. *Cont.*
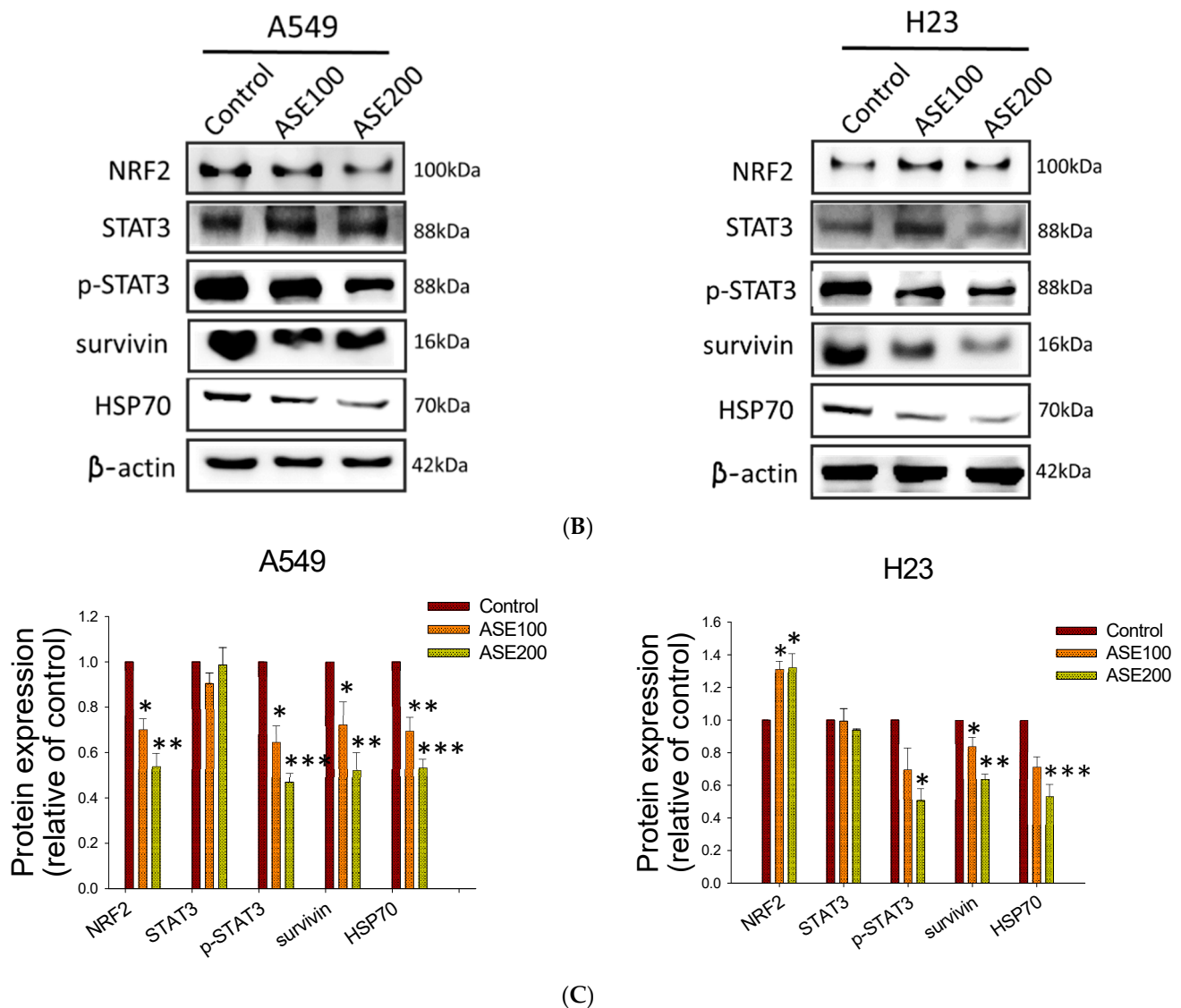
(B)

(C)

Figure 4. Effects of the ethanol extract of *Artemisia santolinifolia* (ASE) on the nuclear factor erythroid-2-related factor 2 (NRF2)/signal transduction and activator of transcription 3 (STAT3) axis and on downstream prosurvival proteins. (**A**) Flow diagram of the ASE-targeted interaction network. (**B**) A549 and H23 cells were treated with the ASE at concentrations of 100 and 200 μg/mL for 48 h. Expression levels of NRF2, STAT3, phosphorylated (p)-STAT3, survivin, and heat shock protein 70 (HSP70) were detected by Western blotting. β-actin was used as a loading control. (**C**) Histograms quantifying of three replicates of Western blot results. Data are the mean ± SE; * $p < 0.05$, ** $p < 0.01$, *** $p < 0.001$ vs. the corresponding control.

3.5. Chemical Profile of ASE

Fresh aerial parts of *A. santolinifolia* were harvested in the eastern part of Mongolia (Omnogobi, Gurvansaikhan, Mongolia). The plant was identified and provided by the traditional herb medicine company, Mong-Em (Ulaanbaatar, Mongolia). The ASE was analyzed by an LC-QToF mass spectrometer. Here, we list the ten most abundant constituents identified in the *A. santolinifolia* whole-plant ethanol extract, with reported potential antitumor activities referenced in previous studies. In our study, procyanidin A2 and nor-ψ-tropine were identified as the dominant constituents in the ASE, followed by hyodeoxycholic acid, nigakilactone H, and siraitic acid C (Table 1). In addition to these findings, the amounts of steroids, flavonoids, and terpenoid contents were evaluated in the whole plant crude extract. For the first time, this investigation reports the identification

of a new nortropane alkaloid, nor-ψ-tropine, from the extract of *A. santolinifolia* using the LC-QToF technique.

Table 1. The main identified constituents of the *Artemisia santolinifolia* ethanol extract (ASE).

No.	Compound Name	Compound Formula	Observed RT (min)	Observed *m/z*	Mass Error (ppm)	Reference
1.	Procyanidin A2	$C_{30}H_{24}O_{12}$	5.56	577.1344	0.6	[34]
2.	Nor-ψ-tropine	$C_8H_{15}NO$	18.97	128.1062	−6.1	-
3.	Hyodeoxycholic acid	$C_{24}H_{40}O_4$	18.54	393.298	−4.9	[35]
4.	Nigakilactone H	$C_{22}H_{32}O_8$	6.69	425.2141	−6.8	[36]
5.	Siraitic acid C	$C_{29}H_{44}O_5$	14.72	441.3018	4.3	-
6.	16-O-Acetylisoiridogermanal	$C_{46}H_{78}O_6$	6.98	517.3895	1.5	-
7.	Blestrianol B	$C_{37}H_{32}O_7$	19.03	589.2231	1.7	-
8.	Biatractylolide	$C_{30}H_{38}O_4$	6.43	463.2882	8.3	[37]
9.	Scutellarin	$C_{21}H_{18}O_{12}$	19.11	449.1113	7.7	[38,39]
10.	Protodiosgenin	$C_{27}H_{42}O_3$	6.33	595.389	8.3	[40]

RT, retention time.

4. Discussion

An expanding number of studies have suggested that various herbs have an enormous yet unexploited potential for anticancer activity. They are appealing candidates for developing modern adjuvant therapeutics to overcome chemoresistance via "multiple molecular mechanisms" and "multi-component and multi-target" manifestations [41]. To date, many studies have shown that active compounds of distinct *Artemisia* species induce apoptosis in cancer cells [42]. Kim et al. demonstrated that an extract of *A. annua* Linné (AAE) exerted apoptotic activities in in vitro and in vivo studies via modulation of phosphoinositide-dependent kinase 1 (PDK1)/Akt signaling pathways [43]. However, we are the first group to demonstrate that the ASE can inhibit the cell viability of NSCLC cells. In agreement with previous studies, the ASE predominantly activated caspase-3 and its cleavage in the H23 cell line, and we propose that cell growth inhibition was correlated with caspase-dependent apoptotic cell death. Surprisingly, the results from Annexin V/7-AAD double-staining pointed out that another mode of cell death prevailed in A549 cells. Our study indicated that the ASE can simultaneously cause multiple forms of tumor cell death, whereby the NSCLC cells could be susceptible to distinct forms of cell death, either apoptosis or iron-dependent programmed ferroptosis.

Artemisinin (ART) is a natural active compound isolated from the traditional Chinese plant *A. annua* and was formerly used as an antimalarial drug. Recently, it was discovered that a semisynthetic derivative of this compound could induce ferroptosis in tumor cells, triggered by iron-dependent lipid peroxidation [44]. ART induces ferroptosis primarily by activating intracellular ROS production in cancer cells, depending on the ferritin level [45]. Several reports pointed out the importance of intracellular free iron concentrations in ferroptosis and proteins involved in iron uptake, storage, and processing that may regulate ferroptosis [46]. In our study, the ASE-induced ROS accumulation and lipid peroxidation prevailed in A549 cells, and these amendments were attenuated when cells were treated with DFO, an iron-chelator. Linking their findings to previous research, Shimada and colleagues discovered that ferroptosis inducers were more cell-line selective than other compounds ($p < 0.01$), allowing the identification of biomarkers that may predict the sensitivity of cells to certain cell death inducers using cell line-selective filters [47]. That might be one prospective explanation relevant to our results that certain cell lines are preferentially sensitive to ASE-induced ferroptosis.

Moreover, many of NRF2′s downstream genes are involved in iron/heme, lipid metabolism, and apoptosis, making it a significant regulator of redox homeostasis [48]. Chen et al. discovered that a root extract of *Beilschmiedia tsangii* (BT extract) is a potential selective regulator of NRF2 signaling and can suppress NRF2 signaling in NRF2-hyperactivated Huh7 cells while activating it in HaCaT cells [49]. The findings from other studies also underscore how the balance of NRF2 protein levels in A549 and H23 cells impacts the overall response to cisplatin therapy, with immunofluorescence images of

NRF2 being strongly expressed in nuclei of A549 cells but dramatically decreased in H23 cells [50].

STAT3 is another proto-oncogenic factor that was reported to be over-activated in around half of all NSCLC cell lines and primary tumors; it stimulates various prosurvival genes such as survivin to protect cells against drug-induced apoptosis [51]. Both NRF2 and STAT3 are antioxidant and cellular stress response factors, and they regulate downstream target ferroptosis-related genes such as solute carrier family 7 member 11 (SLC7A11) of the xCT system to boost cellular resistance to drug-induced death. This indicates that NRF2 and STAT3 might correspond to SLC7A11 expression in ferroptosis, a key gene involved in regulating redox-balancing proteins such as GPX4 [52]. In agreement with previous reports, our study demonstrated that the ASE inhibited NRF2 and GPX4 expressions in A549 cells but slightly increased NRF2 levels in H23 cells, giving the cells a chance to evade oxidative stress. Furthermore, unlike in A549 cells, after the ASE treatment, cleavage of caspase-3 prevailed in H23 cells, suggesting that ASE-induced cell death is possibly potentiated through the induction of apoptosis; at the same time, no significant alterations in the expression of the GPX4 protein or ROS activation were detected.

One of the interesting results of this study also was the evaluation of procyanidin A2 (PCA2) in the ASE for the first time using an LC-QTOF analysis. In regard to specific types of proanthocyanidins, which are a class of flavonoids, several studies documented the anti-inflammatory and antioxidative effects of PCA2. A previous study further showed that PCA2 suppresses ROS by upregulating the expressions of Nrf2 and heme oxygenase (HO)-1, which help protect cancer cells against oxidative stress [53,54]. Additionally, biatractylolide, a double sesquiterpene ester previously isolated from the ethyl acetate extract of *Atractylodes macrocephala*, can effectively attenuate glutamate-induced ROS in PC12 and SH-SY5Y cell lines and showed an anticancer effect [37]. Contrarily, another active constitutive of the ASE, scutellarin, a flavonoid isolated from the traditional Chinese herb *Scutellaria altissima* L., was reported to possess cytotoxic effects against colorectal cancer and bladder cancer cell lines and also exhibited a chemosensitization property in human prostate tumor cells [38,55]. Scutellarin, isolated from the herbal medicine *Erigeron breviscapus*, inhibited the proliferation and promoted apoptosis in A549 cells, concurrently increasing the intracellular ROS level and cleavage of caspase-3, pointing to controversial results of the bioactivities of the abundant constitutes discussed above [56]. To date, ROS-promoting strategies have shown much better anticancer effects and clinical prospects than ROS-reduction strategies, which can be implemented by using an agent that either increases ROS production or reduces the antioxidant capacity of tumor cells [57]. Although increasing evidence shows that natural products can serve as alternative substitutions or additional components of conventional therapies in managing different malignancies, considering the multi-component structure of herbal extracts, interactions and basic pharmacological effects of active ingredients in compounds need to be further studied in order to illustrate their antiproliferative mechanisms of action [57] more clearly.

Collectively, ASE suppressed the STAT3 signaling molecule and downstream molecular targets of survivin and HSP70 in both cell lines, regardless of how it triggers cell death, indicating that the possible anticancer mechanism of action of the ASE is through attenuating prosurvival proteins. Our results also highlight that the molecular mechanisms underlying the susceptibility of NSCLC cells to multiple modes of cell death upon ASE exposure are most likely triggered by the dual role of the NRF2 regulator.

5. Conclusions

Our results revealed that ASE possesses an anticancer activity against NSCLC by inducing multiple cell death modes. This study demonstrated that ASE resulted in caspase-3 cleavage, indicators of apoptosis predominately in H23 cells, while ASE triggered ROS production, lipid peroxidation and altered GPX4 level expression preferentially in A549 cells. Moreover, ASE was found to dual-selectively target the NRF2 signaling molecule aside from downregulating STAT3 along with downstream prosurvival proteins in both

cell lines, suggesting that NRF2 is an essential balance regulator of the antitumor activity of ASE in the simultaneous activating of distinct cell death features.

References

1. Jemal, A.; Siegel, R.; Ward, E.; Hao, Y.; Xu, J.; Thun, M.J. Cancer statistics, 2009. *CA Cancer J. Clin.* **2009**, *59*, 225–249. [CrossRef] [PubMed]
2. Siegel, R.L.; Miller, K.D.; Jemal, A. Cancer statistics, 2016. *CA Cancer J. Clin.* **2016**, *66*, 7–30. [CrossRef] [PubMed]
3. Hardy, D.; Cormier, J.N.; Xing, Y.; Liu, C.C.; Xia, R.; Du, X.L. Chemotherapy-associated toxicity in a large cohort of elderly patients with non-small cell lung cancer. *J. Thorac. Oncol.* **2010**, *5*, 90–98. [CrossRef] [PubMed]
4. Holohan, C.; Van Schaeybroeck, S.; Longley, D.B.; Johnston, P.G. Cancer drug resistance: An evolving paradigm. *Nat. Rev. Cancer* **2013**, *13*, 714–726. [CrossRef]
5. Longley, D.B.; Johnston, P.G. Molecular mechanisms of drug resistance. *J. Pathol.* **2005**, *205*, 275–292. [CrossRef]
6. Mukherjee, P.; Bahadur, S.; Harwansh, R.; Biswas, S.; Banerjee, S. Paradigm shift in natural product research: Traditional medicine inspired approaches. *Phytochem. Rev.* **2016**, *16*, 803–826. [CrossRef]
7. Venkatesha, S.H.; Berman, B.M.; Moudgil, K.D. Herbal medicinal products target defined biochemical and molecular mediators of inflammatory autoimmune arthritis. *Bioorg. Med. Chem.* **2011**, *19*, 21–29. [CrossRef]
8. Nie, J.; Zhao, C.; Deng, L.I.; Chen, J.; Yu, B.; Wu, X.; Pang, P.; Chen, X. Efficacy of traditional Chinese medicine in treating cancer. *Biomed. Rep.* **2016**, *4*, 3–14. [CrossRef]
9. Von Wehrden, H.; Wesche, K.; Miehe, G. Plant communities of the southern Mongolian Gobi. *Phytocoenologia* **2009**, *39*, 331–376. [CrossRef]
10. Wesche, K.; Ronnenberg, K. Phytosociological affinities and habitat preferences of Juniperus sabina L. and Artemisia santolinifolia Turcz. ex Bess. in mountain sites of the south-eastern Gobi Altay, Mongolia. *Feddes Repert. Z. Bot. Taxon. Und Geobot.* **2004**, *115*, 585–600. [CrossRef]
11. Tan, R.X.; Zheng, W.F.; Tang, H.Q. Biologically active substances from the genus Artemisia. *Planta Med.* **1998**, *64*, 295–302. [CrossRef] [PubMed]
12. Watson, L.E.; Bates, P.L.; Evans, T.M.; Unwin, M.M.; Estes, J.R. Molecular phylogeny of Subtribe Artemisiinae (Asteraceae), including Artemisia and its allied and segregate genera. *BMC Evol. Biol.* **2002**, *2*, 17. [CrossRef] [PubMed]
13. Aglarova, A.; Zilfikarov, I.; Severtseva, O. Biological characteristics and useful properties of tarragon (*Artemisia dracunculus* L.). *Pharm. Chem. J.* **2008**, *42*, 81–86. [CrossRef]
14. Hussain, A.; Hayat, M.Q.; Sahreen, S.; Ain, Q.U.; Bokhari, S.A. Pharmacological promises of genus Artemisia (Asteraceae): A review. *Proc. Pak. Acad. Sci. B Life Environ. Sci.* **2017**, *54*, 265–287.
15. Ligaa, U. *Medicinal Plants of Mongolia Used in Mongolian Traditional Medicine*; KCA Press: Seoul, Korea, 1996; pp. 333–334.
16. Choi, E.; Park, H.; Lee, J.; Kim, G. Anticancer, antiobesity, and anti-inflammatory activity of Artemisia species in vitro. *J. Tradit. Chin. Med.* **2013**, *33*, 92–97. [CrossRef]
17. Bora, K.S.; Sharma, A. The genus Artemisia: A comprehensive review. *Pharm. Biol.* **2011**, *49*, 101–109. [CrossRef]
18. Richard, A.J.; Burris, T.P.; Sanchez-Infantes, D.; Wang, Y.; Ribnicky, D.M.; Stephens, J.M. Artemisia extracts activate PPARgamma, promote adipogenesis, and enhance insulin sensitivity in adipose tissue of obese mice. *Nutrition* **2014**, *30*, S31–S36. [CrossRef]
19. Ronnenberg, K. Reproductive ecology of two common woody species, Juniperus sabina and Artemisia santolinifolia, in mountain steppes of southern Mongolia. *Erforsch. Biol. Ressour. Mong.* **2005**, *9*, 207–223.
20. Moulaie, S.; Mirzaie, A.; Aliasgari, E. Antibacterial and anticancer activities of silver nanoparticles fabricated by the Artemisia scoparia extract against lung cancer cell line (A549). *Feyz J. Kashan Univ. Med. Sci.* **2018**, *22*, 487–496.
21. Lian, G.; Li, F.; Yin, Y.; Chen, L.; Yang, J. Herbal extract of Artemisia vulgaris (mugwort) induces antitumor effects in HCT-15 human colon cancer cells via autophagy induction, cell migration suppression and loss of mitochondrial membrane potential. *J. BUON* **2018**, *23*, 73–78.
22. Ali, A.N.M.; Saeed, N.; Omear, H.A. The Anticancer Properties of Artemisia aucheri Boiss Extract on HT29 Colon Cancer Cells. *J. Gastrointest. Cancer* **2021**, *52*, 113–119. [CrossRef] [PubMed]

23.　Lang, S.J.; Schmiech, M.; Hafner, S.; Paetz, C.; Steinborn, C.; Huber, R.; Gaafary, M.E.; Werner, K.; Schmidt, C.Q.; Syrovets, T.; et al. Antitumor activity of an Artemisia annua herbal preparation and identification of active ingredients. *Phytomedicine* **2019**, *62*, 152962. [CrossRef] [PubMed]

24.　Houghton, P.; Fang, R.; Techatanawat, I.; Steventon, G.; Hylands, P.J.; Lee, C.C. The sulphorhodamine (SRB) assay and other approaches to testing plant extracts and derived compounds for activities related to reputed anticancer activity. *Methods* **2007**, *42*, 377–387. [CrossRef] [PubMed]

25.　Liu, Y.K.; Chen, K.H.; Leu, Y.L.; Way, T.D.; Wang, L.W.; Chen, Y.J.; Liu, Y.M. Ethanol extracts of Cinnamomum kanehirai Hayata leaves induce apoptosis in human hepatoma cell through caspase-3 cascade. *Onco Targets Ther.* **2015**, *8*, 99–109. [CrossRef] [PubMed]

26.　Dixon, S.J.; Lemberg, K.M.; Lamprecht, M.R.; Skouta, R.; Zaitsev, E.M.; Gleason, C.E.; Patel, D.N.; Bauer, A.J.; Cantley, A.M.; Yang, W.S.; et al. Ferroptosis: An iron-dependent form of nonapoptotic cell death. *Cell* **2012**, *149*, 1060–1072. [CrossRef] [PubMed]

27.　Tang, H.M.; Tang, H.L. Cell recovery by reversal of ferroptosis. *Biol. Open* **2019**, *8*, bio043182. [CrossRef] [PubMed]

28.　Efferth, T. From ancient herb to modern drug: Artemisia annua and artemisinin for cancer therapy. *Semin. Cancer Biol.* **2017**, *46*, 65–83. [CrossRef]

29.　Li, J.; Cao, F.; Yin, H.L.; Huang, Z.J.; Lin, Z.T.; Mao, N.; Sun, B.; Wang, G. Ferroptosis: Past, present and future. *Cell Death Dis.* **2020**, *11*, 88. [CrossRef]

30.　Proneth, B.; Conrad, M. Ferroptosis and necroinflammation, a yet poorly explored link. *Cell Death Differ.* **2019**, *26*, 14–24. [CrossRef]

31.　Thayyullathil, F.; Cheratta, A.R.; Alakkal, A.; Subburayan, K.; Pallichankandy, S.; Hannun, Y.A.; Galadari, S. Acid sphingomyelinase-dependent autophagic degradation of GPX4 is critical for the execution of ferroptosis. *Cell Death Dis.* **2021**, *12*, 26. [CrossRef]

32.　Wang, D.; Zhong, B.; Li, Y.; Liu, X. Dihydroartemisinin increases apoptosis of colon cancer cells through targeting Janus kinase 2/signal transducer and activator of transcription 3 signaling. *Oncol. Lett.* **2018**, *15*, 1949–1954. [CrossRef] [PubMed]

33.　Liu, Q.; Wang, K. The induction of ferroptosis by impairing STAT3/Nrf2/GPx4 signaling enhances the sensitivity of osteosarcoma cells to cisplatin. *Cell Biol. Int.* **2019**, *43*, 1245–1256. [CrossRef] [PubMed]

34.　Minker, C.; Duban, L.; Karas, D.; Jarvinen, P.; Lobstein, A.; Muller, C.D. Impact of Procyanidins from Different Berries on Caspase 8 Activation in Colon Cancer. *Oxid. Med. Cell. Longev.* **2015**, *2015*, 154164. [CrossRef] [PubMed]

35.　Im, E.; Martinez, J.D. Ursodeoxycholic acid (UDCA) can inhibit deoxycholic acid (DCA)-induced apoptosis via modulation of EGFR/Raf-1/ERK signaling in human colon cancer cells. *J. Nutr.* **2004**, *134*, 483–486. [CrossRef] [PubMed]

36.　Yan, Z.; Guo, G.F.; Zhang, B. Research of Brucea javanica against cancer. *Chin. J. Integr. Med.* **2017**, *23*, 153–160. [CrossRef] [PubMed]

37.　Zhu, L.; Ning, N.; Li, Y.; Zhang, Q.F.; Xie, Y.C.; Irshad, M.; Feng, X.; Tao, X.J. Biatractylolide Modulates PI3K-Akt-GSK3beta-Dependent Pathways to Protect against Glutamate-Induced Cell Damage in PC12 and SH-SY5Y Cells. *Evid. Based Complement. Altern. Med.* **2017**, *2017*, 1291458. [CrossRef]

38.　Gao, C.; Zhou, Y.; Jiang, Z.; Zhao, Y.; Zhang, D.; Cong, X.; Cao, R.; Li, H.; Tian, W. Cytotoxic and chemosensitization effects of Scutellarin from traditional Chinese herb *Scutellaria altissima* L. in human prostate cancer cells. *Oncol. Rep.* **2017**, *38*, 1491–1499. [CrossRef]

39.　Xu, H.; Zhang, S. Scutellarin-induced apoptosis in HepG2 hepatocellular carcinoma cells via a STAT3 pathway. *Phytother. Res.* **2013**, *27*, 1524–1528. [CrossRef]

40.　Kim, D.S.; Jeon, B.K.; Lee, Y.E.; Woo, W.H.; Mun, Y.J. Diosgenin Induces Apoptosis in HepG2 Cells through Generation of Reactive Oxygen Species and Mitochondrial Pathway. *Evid. Based Complement. Altern. Med.* **2012**, *2012*, 981675. [CrossRef]

41.　Guo, W.; Tan, H.Y.; Chen, F.; Wang, N.; Feng, Y. Targeting Cancer Metabolism to Resensitize Chemotherapy: Potential Development of Cancer Chemosensitizers from Traditional Chinese Medicines. *Cancers* **2020**, *12*, 404. [CrossRef]

42.　Ahmadi, F.; Mojarrab, M.; Ghazi-Khansari, M.; Hosseinzadeh, L. A semipolar fraction of petroleum ether extract of Artemisia aucheri induces apoptosis and enhances the apoptotic response to doxorubicin in human neuroblastoma SKNMC cell line. *Res. Pharm. Sci.* **2015**, *10*, 335–344. [PubMed]

43.　Kim, E.J.; Kim, G.T.; Kim, B.M.; Lim, E.G.; Kim, S.Y.; Kim, Y.M. Apoptosis-induced effects of extract from Artemisia annua Linne by modulating PTEN/p53/PDK1/Akt/ signal pathways through PTEN/p53-independent manner in HCT116 colon cancer cells. *BMC Complement. Altern. Med.* **2017**, *17*, 236. [CrossRef] [PubMed]

44.　Ooko, E.; Saeed, M.E.; Kadioglu, O.; Sarvi, S.; Colak, M.; Elmasaoudi, K.; Janah, R.; Greten, H.J.; Efferth, T. Artemisinin derivatives induce iron-dependent cell death (ferroptosis) in tumor cells. *Phytomedicine* **2015**, *22*, 1045–1054. [CrossRef] [PubMed]

45.　Zhu, S.; Yu, Q.; Huo, C.; Li, Y.; He, L.; Ran, B.; Chen, J.; Li, Y.; Liu, W. Ferroptosis: A Novel Mechanism of Artemisinin and its Derivatives in Cancer Therapy. *Curr. Med. Chem.* **2021**, *28*, 329–345. [CrossRef]

46.　Lei, P.; Bai, T.; Sun, Y. Mechanisms of Ferroptosis and Relations With Regulated Cell Death: A Review. *Front. Physiol.* **2019**, *10*, 139. [CrossRef] [PubMed]

47.　Shimada, K.; Hayano, M.; Pagano, N.C.; Stockwell, B.R. Cell-Line Selectivity Improves the Predictive Power of Pharmacogenomic Analyses and Helps Identify NADPH as Biomarker for Ferroptosis Sensitivity. *Cell Chem. Biol.* **2016**, *23*, 225–235. [CrossRef] [PubMed]

48. Dodson, M.; Castro-Portuguez, R.; Zhang, D.D. NRF2 plays a critical role in mitigating lipid peroxidation and ferroptosis. *Redox Biol.* **2019**, *23*, 101107. [CrossRef]

49. Xu, H.; Zhang, Y.; Wang, P.; Zhang, J.; Chen, H.; Zhang, L.; Du, X.; Zhao, C.; Wu, D.; Liu, F.; et al. A comprehensive review of integrative pharmacology-based investigation: A paradigm shift in traditional Chinese medicine. *Acta Pharm. Sin. B* **2021**, *11*, 1379–1399. [CrossRef]

50. Silva, M.M.; Rocha, C.R.R.; Kinker, G.S.; Pelegrini, A.L.; Menck, C.F.M. The balance between NRF2/GSH antioxidant mediated pathway and DNA repair modulates cisplatin resistance in lung cancer cells. *Sci. Rep.* **2019**, *9*, 17639. [CrossRef]

51. Barry, S.P.; Townsend, P.A.; McCormick, J.; Knight, R.A.; Scarabelli, T.M.; Latchman, D.S.; Stephanou, A. STAT3 deletion sensitizes cells to oxidative stress. *Biochem. Biophys. Res. Commun.* **2009**, *385*, 324–329. [CrossRef]

52. Qiang, Z.; Dong, H.; Xia, Y.; Chai, D.; Hu, R.; Jiang, H. Nrf2 and STAT3 Alleviates Ferroptosis-Mediated IIR-ALI by Regulating SLC7A11. *Oxid. Med. Cell. Longev.* **2020**, *2020*, 5146982. [CrossRef] [PubMed]

53. Wang, Q.Q.; Gao, H.; Yuan, R.; Han, S.; Li, X.X.; Tang, M.; Dong, B.; Li, J.X.; Zhao, L.C.; Feng, J.; et al. Procyanidin A2, a polyphenolic compound, exerts anti-inflammatory and anti-oxidative activity in lipopolysaccharide-stimulated RAW264.7 cells. *PLoS ONE* **2020**, *15*, e0237017. [CrossRef] [PubMed]

54. Xu, H.-Y.; Feng, X.-H.; Zhao, P.-F.; Damirin, A.; Ma, C.-M. Procyanidin A2 penetrates L-02 cells and protects against tert-butyl hydroperoxide-induced oxidative stress by activating Nrf2 through JNK and p38 phosphorylation. *J. Funct. Foods* **2019**, *62*, 103562. [CrossRef]

55. Lv, W.L.; Liu, Q.; An, J.H.; Song, X.Y. Scutellarin inhibits hypoxia-induced epithelial-mesenchymal transition in bladder cancer cells. *J. Cell. Physiol.* **2019**, *234*, 23169–23175. [CrossRef] [PubMed]

56. Zhang, G.Y.; Chen, W.Y.; Li, X.B.; Ke, H.; Zhou, X.L. Scutellarin-induced A549 cell apoptosis depends on activation of the transforming growth factor-beta1/smad2/ROS/caspase-3 pathway. *Open Life Sci.* **2021**, *16*, 961–968. [CrossRef]

57. Qian, Q.; Chen, W.; Cao, Y.; Cao, Q.; Cui, Y.; Li, Y.; Wu, J. Targeting Reactive Oxygen Species in Cancer via Chinese Herbal Medicine. *Oxid. Med. Cell. Longev.* **2019**, *2019*, 9240426. [CrossRef]